

body in sharks and a regionalized body with a pivoting neck joint and rigid trunk armor in arthrodires. Their evolutionary importance hinges on whether eubranchyothoracid musculature is specialized or primitive relative to that of sharks. Placoderms appear to be a paraphyletic segment of the gnathostome stem group (3, 4), so if any components of eubranchyothoracid musculature can be shown to be general for placoderms, they can also be inferred to be primitive relative to the crown group. The status of the shallow myoseptal curvature cannot yet be determined in this regard, but the muscles of the neck joint and abdomen have specific skeletal associations that allow such phylogenetic inferences to be drawn.

Most ostracoderms, a grade of jawless stem gnathostomes (2) (Fig. 1A), have head shields that also encompass the shoulder-girdle region (2). This suggests that the gnathostome shoulder girdle originated through subdivision of the shield. Almost all placoderms have a mobile joint between the skull and shoulder girdle, implying the need for elevator and depressor muscles such as those observed in eubranchyothoracids. Thus, a cucullaris operating this joint, antagonistic to specialized epaxial head elevators, is probably primitive relative to the crown gnathostome condition of a cucullaris without specialized antagonists that forms part of a broadly flexible neck.

The transverse abdominal muscles of eubranchyothoracids are not as directly tied to a skeletal structure with an identifiable mechanical function. Comparison with those of a recent elephant shark indicates that these muscles are not homologous with any muscles of the pelvic fin or male clasper (supplementary text). However, the transverse abdominals may modulate shear forces between the armor and the laterally undulating body during tail-propelled swimming. A long ventral armor is also present in antiarchs, recovered as the most primitive placoderms in several recent analyses (3, 4, 15). Transverse abdominal muscles may thus be an attribute of the placoderm segment of the gnathostome stem group and, hence, primitive relative to the absence of such muscles at the base of the gnathostome crown group.

Outside of placoderms, transversely oriented abdominal muscle fibers are restricted to tetrapods and have been regarded as a tetrapod autapomorphy (16). Their associated connective tissues and tendons are derived from the somatopleure component of the lateral plate mesoderm (17), which plays an important role in hypaxial myogenesis (18). In lampreys, the posterior lateral plate mesoderm is not separated into splanchnic and somatopleuric components (19), meaning that it cannot give rise to somatopleure-derived structures such as paired fins. The presence of paired fins in placoderms shows that separation of somatopleure and splanchnopleure had occurred, supporting the inference that their transverse muscles may have been patterned by

the same somatopleure-based mechanism as in tetrapods.

The arthrodires of the Gogo Formation reveal an elaborate regionalized musculature, including the earliest and phylogenetically deepest examples of several muscle types. Particularly surprising is the extensive development of transverse-fiber muscles in the ventral body wall, which parallels the condition in tetrapods. Hypothetical reconstructions are not able to recover the full complexity of this musculature, either on the basis of biomechanical analysis or phylogenetic bracketing, and are thus liable to give a false picture of muscular evolution at the origin of gnathostomes. The study of exceptionally preserved fossils will continue to provide essential data for the reconstruction of vertebrate soft anatomy, particularly in groups with no close living relatives.

#### References and Notes

1. Y. Oisi, K. G. Ota, S. Kuraku, S. Kuratani, *Nature* **493**, 175–180 (2013).
2. P. Janvier, *Early Vertebrates* (Clarendon Press, Oxford, 1996).
3. M. D. Brazeau, *Nature* **457**, 305–308 (2009).
4. S. P. Davis, J. A. Finarelli, M. I. Coates, *Nature* **486**, 247–250 (2012).
5. T. Matsuoka *et al.*, *Nature* **436**, 347–355 (2005).
6. J. Mallatt, *Zool. J. Linn. Soc.* **117**, 329–404 (1996).
7. S. Kuratani, *J. Anat.* **205**, 335–347 (2004).
8. S. Kuratani, *Dev. Growth Differ.* **50** (suppl. 1), S189–S194 (2008).
9. A. Heintz, in *The Bashford Dean Memorial Volume: Archaic Fishes*, E. W. Gudger, Ed. (American Museum of Natural History, New York, 1930), pp. 115–224.
10. R. Miles, T. S. Westoll, *Trans. R. Soc. Edinb.* **67**, 373–476 (1968).
11. F. H. Edgeworth, *The Cranial Muscles of Vertebrates* (Cambridge Univ. Press, Cambridge, 1935).
12. K. Trinajstić, C. Marshall, J. Long, K. Bifield, *Biol. Lett.* **3**, 197–200 (2007).

13. S. Gemballa *et al.*, *Proc. Biol. Sci.* **270**, 1229–1235 (2003).
14. S. A. Wainwright, F. Vosburgh, J. H. Hebrank, *Science* **202**, 747–749 (1978).
15. M. Zhu, X. Yu, B. Choo, J. Wang, L. Jia, *Biol. Lett.* **8**, 453–456 (2012).
16. N. Schilling, *Front. Zool.* **8**, 4 (2011).
17. B. Christ, M. Jacob, H. J. Jacob, *Anat. Embryol.* **166**, 87–101 (1983).
18. S. J. Mathew *et al.*, *Development* **138**, 371–384 (2011).
19. K. Onimaru, E. Shoguchi, S. Kuratani, M. Tanaka, *Dev. Biol.* **359**, 124–136 (2011).

**Acknowledgments:** We acknowledge M. Siverson at the Western Australian Museum, Perth, and Z. Johanson at the Natural History Museum, London, for lending us specimens in their care. We thank I. Montero Verdú for his picture of the muscle bundles (Fig. 3D) and A. Ritchie for an *Eastmanosteus* image. K.T., P.E.A., and C.B. are supported by Australian Research Council (ARC) QEII Fellowship DP 110101127; J.L., K.T., T.S., and G.Y. by ARC DP 1092870; S.S., V.D., and P.E.A. by European Research Council Advanced Investigator Grant 233111; P.E.A. by a Wallenberg Scholarship from the Knut and Alice Wallenberg Foundation; and C.B. by a Human Frontiers Research Program and an ARC Discovery Project, DP 1096002. The scan performed at the European Synchrotron Radiation Facility in Grenoble, France, was part of project EC770. K.T. acknowledges the 2010 Prime Minister's Science Prize, and J.L. acknowledges funding from The Australian Geographic Society, which supported fieldwork at the Gogo Formation. Specimens are housed in the collections of the Western Australian Museum, Australian National University, Australian Museum, and Museum Victoria, Australia, and the Natural History Museum, UK.

#### Supplementary Materials

www.sciencemag.org/cgi/content/full/science.1237275/DC1  
Materials and Methods  
Supplementary Text  
Figs. S1 to S4  
References (20–30)  
Movie S1

4 March 2013; accepted 29 May 2013  
Published online 13 June 2013;  
10.1126/science.1237275

## Enhanced Remote Earthquake Triggering at Fluid-Injection Sites in the Midwestern United States

Nicholas J. van der Elst,<sup>1\*</sup> Heather M. Savage,<sup>1</sup> Katie M. Keranen,<sup>2†</sup> Geoffrey A. Abers<sup>1</sup>

A recent dramatic increase in seismicity in the midwestern United States may be related to increases in deep wastewater injection. Here, we demonstrate that areas with suspected anthropogenic earthquakes are also more susceptible to earthquake-triggering from natural transient stresses generated by the seismic waves of large remote earthquakes. Enhanced triggering susceptibility suggests the presence of critically loaded faults and potentially high fluid pressures. Sensitivity to remote triggering is most clearly seen in sites with a long delay between the start of injection and the onset of seismicity and in regions that went on to host moderate magnitude earthquakes within 6 to 20 months. Triggering in induced seismic zones could therefore be an indicator that fluid injection has brought the fault system to a critical state.

**E**arthquakes can be induced by underground fluid injection, which increases pore pressure and allows faults to slide under pre-existing shear stress (1). The increase in wastewater

disposal from natural gas development and other sources has been accompanied by an increase in fluid-induced earthquakes in recent years (2). These earthquakes include widely felt earthquakes in

Oklahoma, Arkansas, Ohio, Texas, and Colorado (Fig. 1) (3–7). Although most injection wells are not associated with large earthquakes, the converse is not true. At least half of the 4.5 moment magnitude ( $M_w$ ) or larger earthquakes to strike the interior of the United States in the past decade have occurred in regions of potential injection-induced seismicity (table S1). In some cases, the onset of seismicity follows injection by only days or weeks (1, 3, 5), and the association with pumping at particular wells is clear. In others, seismicity increases only after months or years of active injection (4, 8, 9).

A long delay before seismic activation implies that faults may be moving toward a critical state for years before failure. However, currently there are no reliable methods to determine whether a particular field has reached a critical state other than by simply observing a large increase in seismicity. This lack of diagnostics is a key problem in developing operational strategies to mitigate anthropogenic activity (2).

Because induced seismic zones are brought to failure by increased pore pressures, we examined whether areas of induced seismicity show a high susceptibility to dynamic triggering by the small transient stresses carried by seismic waves from distant earthquakes. Dynamic triggering in natural settings has been linked to the presence of subsurface fluids, and seismicity rate changes have been shown to depend systematically on the perturbation stress (10–13). This suggests that dynamic triggering could serve as a probe of the state of stress in areas of wastewater injection. We refer to earthquakes that are promoted by anthropogenic activity as induced and to earthquakes that are initiated by transient natural stresses as triggered. By this definition, there can be triggered induced earthquakes.

A search of the Advanced National Seismic System (ANSS) earthquake catalog gives preliminary evidence that induced seismic zones are sensitive to dynamic triggering by surface waves (Fig. 1). Regions of suspected induced seismicity showed a pronounced increase in 3.0  $M$  and larger earthquakes spanning at least a 3-day window after large ( $M_w \geq 8.6$ ) remote earthquakes: the 27 February 2010 8.8  $M_w$  Maule, Chile; 11 March 2011 9.1  $M_w$  Tohoku-oki; and 12 April 2012 8.6  $M_w$  Sumatra earthquakes. The broader central United States shows essentially no response to these events (Fig. 1). Most of the triggering is at three sites: Prague, Oklahoma; Snyder, Texas; and Trinidad, Colorado. Suggestively, each of these regions went on to host mod-

erate to large earthquakes (4.3 to 5.7  $M_w$ ) within 6 to 20 months of the strong triggering.

Although the triggering is significant at the 96% level (table S2), a closer investigation is warranted. We therefore enhanced the catalog by applying a single-station matched filter to continuous waveforms (14). The matched-filter approach identifies small, uncataloged earthquakes based on their similarity to target events (15–17). Distinct families of earthquakes are distinguished based on the difference in  $P$  and  $S$  wave travel times ( $S-P$  time), which gives the approximate radial distance from the seismic station (15).

The Cogdell oil field (8), located near Snyder, Texas, hosted a seismic swarm in September 2011 that included a 4.3  $M_w$  main shock (supplementary text). The enhanced catalog shows that the Tohoku-oki earthquake triggered a significant number of earthquakes (14) at this site (Fig. 2 and table S2). In fact, the rate of earthquakes within the 10 days after the Tohoku-oki earthquake was the highest observed over the entire study duration (February 2009 to present), excluding the days immediately after the 4.3  $M_w$  main shock. The triggered earthquakes show a swarm like signature, typical of fluid-induced earthquakes (18), with the largest of the triggered events (3.8  $M_w$ , ANSS) occurring after 2.5 days of smaller events (Fig. 2C). The much earlier February 2010 Maule earthquake did not trigger at Snyder, nor did the post-swarm April 2012 Sumatra earthquake.

Prague, Oklahoma, experienced three 5.0  $M_w$  and greater earthquakes in November 2011, associated with fluid disposal in the Wilzetta field (supplementary text) (4). The enhanced catalog shows that the February 2010 Maule event triggered a strong sequence of earthquakes near the eventual epicenter of the first 5.0  $M_w$  earthquake (Fig. 3 and table S2). The rate of earthquakes in the several days after the Maule trigger far

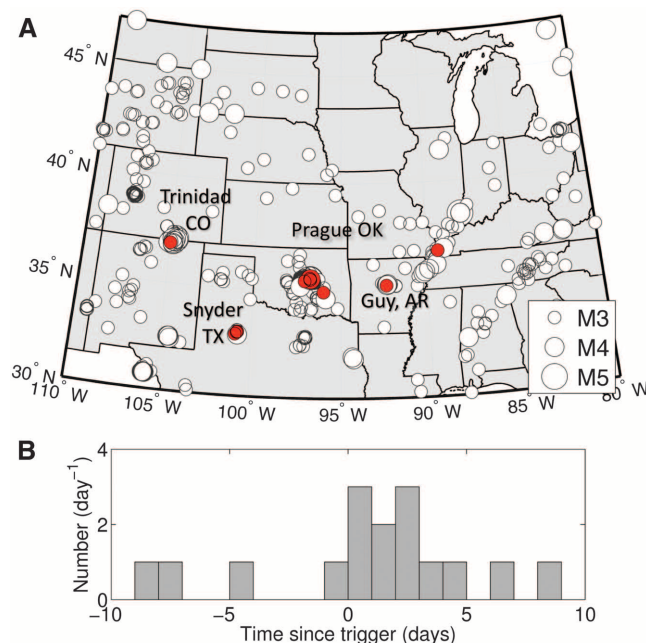
exceeds that of any other time within the period of observation, up to the  $M_w \geq 5.0$  earthquakes themselves, which is similar to the observation at Snyder. There are no events detected within  $\pm 32$  km relative distance for at least 4 months before the 2010 Maule earthquake.

The largest event in the remotely triggered sequence is a 4.1  $M_w$ , 16 hours after the 2010 Maule earthquake, which may account for the large number of earthquakes that continued up to the time of the first 5  $M_w$  Prague earthquake in 2011 (Fig. 3). If the 4.1  $M_w$  earthquake can be considered a foreshock of the subsequent 5.7  $M_w$  Prague earthquake, then the 5.7  $M_w$  event is not only one of the largest earthquakes to be associated with wastewater disposal (2) but also one of the largest earthquakes to be linked indirectly to a remote triggering event (4, 19).

The April 2011 Tohoku-oki earthquake, which occurred during the ongoing sequence before the 5.7  $M_w$  Prague main shock, did not trigger additional earthquakes near the swarm (Fig. 3 and table S2). The 2012 Sumatra earthquake, on the other hand, followed the main 5.7  $M_w$  Prague earthquake by 5 months and triggered a small uptick in activity that was consistent with the far northeastern tip of the swarm (Fig. 3C). However, this triggered rate change is much smaller than that triggered by the Maule earthquake in 2010.

Trinidad, Colorado, experienced a seismic swarm in August 2011 that included a 5.3  $M_w$  main shock, possibly related to coal-bed methane extraction and reinjection of the produced water in the Raton Basin (supplementary text). The February 2010 Maule earthquake triggered a small but statistically significant response near the site of the 5.3  $M_w$  main shock (Fig. 4 and table S2). Although the total number of triggered events is small (four), the binomial probability of observ-

**Fig. 1. Remote triggering in the midwestern United States, from the composite ANSS catalog. (A)** Cataloged earthquakes above 3.0  $M$  between 2003 and 2013 (ANSS). Earthquakes in red occurred during the first 10 days after the February 2010, Maule; March 2011, Tohoku-oki; or April 2012, Sumatra earthquakes. Triggering occurs almost exclusively in three injection fields, labeled Prague, Trinidad, and Snyder. **(B)** Stacked earthquake counts in the 10 days before and after the three  $\geq 8.6$   $M_w$  remote earthquakes. The histogram excludes the Guy, Arkansas, swarm, which dominates event rates at the time of the 2011 Tohoku-oki earthquake but did not trigger (supplementary text).



<sup>1</sup>Lamont-Doherty Earth Observatory of Columbia University, Post Office Box 1000, 61 Route 9W, Palisades, NY 10964, USA.

<sup>2</sup>ConocoPhillips School of Geology and Geophysics, University of Oklahoma, 100 East Boyd Street, Norman, OK 73069, USA.

\*Corresponding author. E-mail: nicholas@ldeo.columbia.edu

†Present address: Department of Earth and Atmospheric Sciences, Cornell University, 410 Thurston Avenue, Ithaca, NY 14850, USA.

**Fig. 2. Matched-filter enhanced catalog for Snyder, Texas.** (A) Detected events, showing triggering by the 2011 Tohoku-oki earthquake. Symbols along top show strength of triggering (red, strong; green, none). Red star marks 11 September 2011 4.3  $M_w$  main shock (NEIC catalog). Colors correspond to station in (B), with ANSS catalog in gray. Seismometer operating times and the times at which we have enhanced the catalog are shown by thin and thick horizontal bars, respectively. (B) Mapped distances to detected events. Small circles are ANSS catalog earthquakes; a red star shows the main shock. Yellow squares are nearby active injection wells. (C) Cumulative event count around the 2010 Maule and 2011 Tohoku-oki earthquakes.

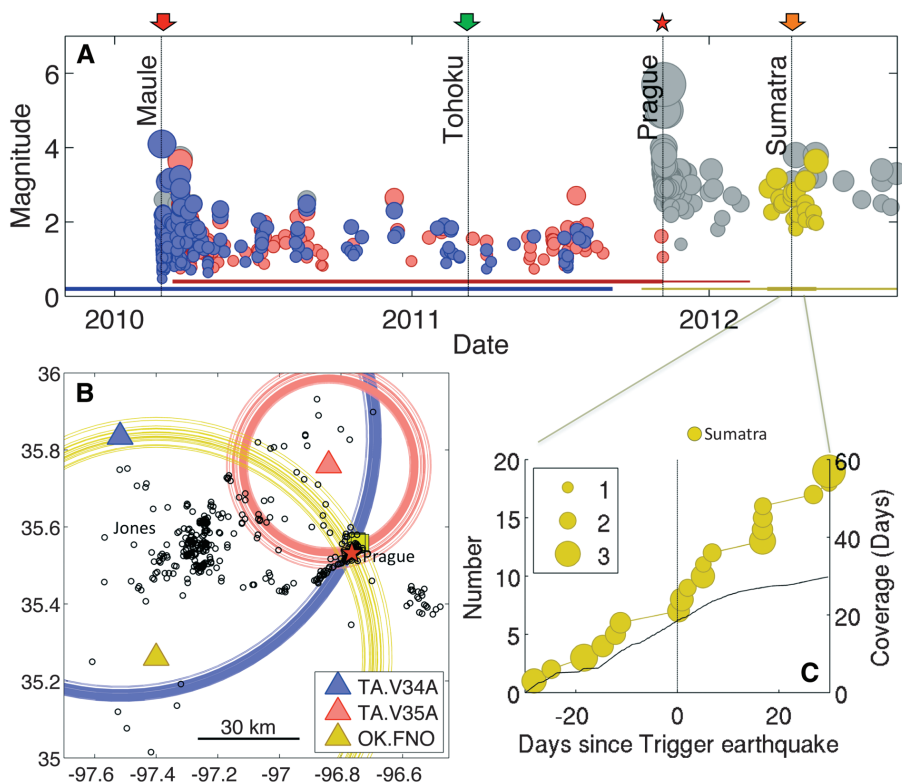
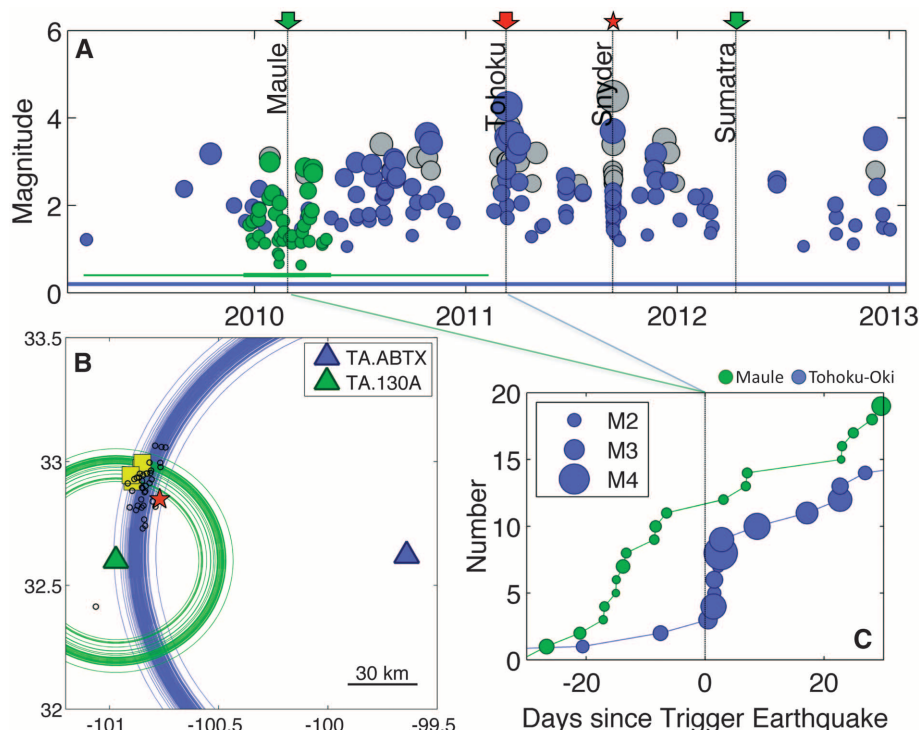


**Fig. 3. Matched-filter enhanced catalog for Prague, Oklahoma.** (A) Detected events, showing triggering by the 2010 Maule earthquake. Red star marks the 6 November 2011 5.7  $M_w$  main shock. Other details are as in Fig. 2A. (B) Mapped distances to detected events. Details are as in Fig. 2B. (C) Cumulative event count around the 2012 Sumatra earthquake. Cumulative recording time for this intermittently operating station is shown over the same period.

ing this many events in 1 day after the trigger, given five events in the entire previous year, is less than  $10^{-5}$ .

The March 2011 Tohoku-oki earthquake, which occurred during the active portion of the swarm, did not trigger additional seismicity at Trinidad. The

2012 Sumatra earthquake occurred 8 months after the 5.3  $M_w$  Trinidad main shock and triggered a moderate surge in activity that was consistent with the far edge of the swarm, where previous swarm activity had not occurred (fig. S2). This pattern—strong triggering by the first remote earthquake, none by the second, and marginal triggering after the swarm—is very similar to that observed in Oklahoma.

We examined several other regions in the United States that have experienced moderate magnitude earthquakes or heightened seismicity rates linked to fluid injection, including Guy, Arkansas; Jones, Oklahoma; and Youngstown, Ohio. None of these other regions appear to have responded to remote triggering (supplementary text).

The strongly triggered regions were exceptional in that they had a long history of pumping within 10 km of the eventual swarms yet were relatively quiet for much of that history. At other sites of induced moderate earthquakes (Guy, Arkansas, and Youngstown, Ohio), the lag time between the start of pumping and onset of seismicity was as little as months or weeks, presenting a relatively small window of vulnerability to dynamic triggering before the swarms.

The delay in induced seismicity in some regions could be due to complexities in the local geology (supplementary text). In Oklahoma, injection occurred into a fault-bounded pocket, and pressures may have built up slowly over time because of the size of the reservoir bounded by impermeable faults (4). The Cogdell field may have similar isolated pockets, formed by discrete carbonate reefs buried within impermeable shales (8).

Fluids have been suggested as an important component in dynamic triggering since early

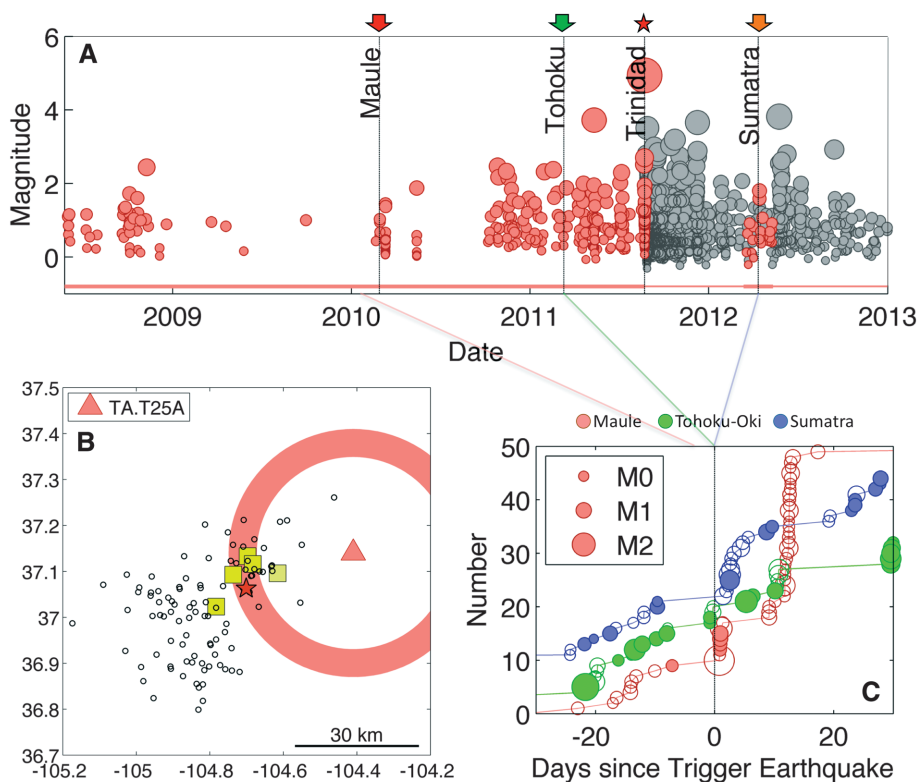


**Fig. 4. Matched-filter enhanced catalog for Trinidad, Colorado.** (A) Detected events, showing triggering by the 2010 Maule earthquake. Red star marks the 23 August 2011 5.3  $M_w$  main shock. Other details are as in Fig. 2A. (B) Mapped distances to detected events. Details are as in Fig. 2B. (C) Waveform detection counts around the 2010 Maule, 2011 Tohoku-oki, and 2012 Sumatra earthquakes (curves offset for clarity). Filled circles are within 2.5-km radial distance relative to the 5.3  $M_w$  main shock, and open circles are within ~5 km (fig. S2).

observations showed preferential triggering in active volcanic and hydrothermal systems (13, 20, 21). Some features of our observations are also suggestive of a fluid mechanism for triggering. First, in all of the studied cases the triggered earthquakes occurred with a small delay with respect to the passage of the seismic waves, initiating within less than 24 hours and continuing for days to months afterward. This pattern suggests a triggering mechanism that relies on dynamic permeability enhancement and transport of fluids (22, 23), as has been suggested for natural triggered seismicity (20–22). In this scenario, stress transients alter the permeability of hydraulic conduits in the reservoir, accelerating diffusion of pore pressure into local faults. Fractures in active injection reservoirs may be particularly susceptible to this mechanism because the injection of unequilibrated fluids may lead to clogging through mineralization and sedimentation. A brief pressure transient may then flush out these clogged fractures (22, 24).

In Prague and Trinidad, only the first of two large remote events caused earthquakes, despite imparting dilational and shear strains that are similar to subsequent events (table S4). This is also consistent with the permeability enhancement model, which requires a certain amount of recharge time between triggering episodes (24). After local fault slip is triggered, the local permeability rises dra-

matically because of microfracturing and dilation (25), promoting further fluid diffusion over several rupture dimensions (26). Hence, once the seismic swarm is underway the fractures may not return to a state in which they are susceptible to unclogging by small transient stresses.

We find that certain areas of fluid injection are sensitive to small changes in stress associated with the passage of seismic waves from remote large earthquakes. The observations suggest several requirements for an induced region to be sensitive to remote triggering. First, all of the triggered sites in this study had a long history of regional subsurface injection over a period of decades. Second, each triggered site was near to hosting a moderate magnitude earthquake, suggesting critically stressed faults. Last, each site had relatively low levels of seismicity rate in the immediate vicinity (10 km) before the first triggering episode. Remote triggering can therefore indicate that conditions within an injection field have crossed some critical threshold, and a larger induced earthquake could be possible or even likely. This underlines the importance of improved seismic monitoring in areas of subsurface fluid injection.

#### References and Notes

1. C. B. Raleigh, J. H. Healy, J. D. Bredehoeft, *Science* **191**, 1230–1237 (1976).

2. National Research Council, *Induced Seismicity Potential in Energy Technologies* (National Academies Press, New York, 2012).
3. S. Horton, *Seismol. Res. Lett.* **83**, 250–260 (2012).
4. K. M. Keranen, H. M. Savage, G. A. Abers, E. S. Cochran, *Geology* **41**, 699–702 (2013).
5. W.-Y. Kim, “Induced seismicity associated with fluid injection into deep wells in Youngstown, Ohio,” abstract S43D-2496 presented at 2012 Fall Meeting, American Geophysical Union, San Francisco, CA, 3 to 7 December 2012.
6. C. Frohlich, J. Glidewell, M. Brunt, *Bull. Seismol. Soc. Am.* **102**, 457–466 (2012).
7. J. L. Rubinstein, W. L. Ellsworth, A. McGarr, “The 2001–present triggered seismicity sequence in the Raton basin of southern Colorado/Northern New Mexico,” BSSA Abstracts 2013 Annual Meeting 155D, (2013).
8. S. D. Davis, W. D. Pennington, *Bull. Seismol. Soc. Am.* **79**, 1477–1494 (1989).
9. R. B. Horner, J. E. Barclay, J. M. MacRae, *Can. J. Explor. Geophys.* **30**, 39–50 (1994).
10. N. J. van der Elst, E. E. Brodsky, *J. Geophys. Res.* **115**, B07311 (2010).
11. H. M. Savage, C. Marone, *J. Geophys. Res.* **113**, B05302 (2008).
12. D. P. Hill, S. G. Prejean, in *Dynamic Triggering*, vol. 4, H. Kanamori, Ed., Treatise on (Elsevier, New York, 2007), pp. 257 to 292.
13. D. P. Hill et al., *Science* **260**, 1617–1623 (1993).
14. Materials and methods are available as supplementary materials on Science Online.
15. C. Frohlich, C. Hayward, B. Stump, E. Potter, *Bull. Seismol. Soc. Am.* **101**, 327–340 (2011).
16. Z. G. Peng, P. Zhao, *Nat. Geosci.* **2**, 877–881 (2009).
17. D. R. Shelly, G. C. Beroza, S. Ide, *Nature* **446**, 305–307 (2007).
18. J. E. Vidale, P. M. Shearer, *J. Geophys. Res.* **111**, B05312 (2006).
19. T. Parsons, A. A. Velasco, *Nat. Geosci.* **4**, 312–316 (2011).
20. E. E. Brodsky, S. G. Prejean, *J. Geophys. Res.* **110**, B04302 (2005).
21. S. Husen, R. Taylor, R. B. Smith, H. Healeser, *Geology* **32**, 537–540 (2004).
22. E. E. Brodsky, E. Roeloffs, D. Woodcock, I. Gall, M. Manga, *J. Geophys. Res.* **108**, (B8), 2390 (2003).
23. T. Taira, P. G. Silver, F. L. Niu, R. M. Nadeau, *Nature* **461**, 636–639 (2009).
24. J. E. Elkhoury, A. Niemeijer, E. E. Brodsky, C. Marone, *J. Geophys. Res.* **116**, (B2), B02311 (2011).
25. T. M. Mitchell, D. R. Faulkner, *J. Geophys. Res.* **113**, (B11), B11412 (2008).
26. S. Micklethwaite, S. F. Cox, *Earth Planet. Sci. Lett.* **250**, 318–330 (2006).

**Acknowledgments:** This paper benefitted from discussions with E. Brodsky and W.-Y. Kim. Injection data for Cogdell Oilfield was provided by C. Frohlich. The Oklahoma Corporation Commission, the Texas Railroad Commission, and the Colorado Oil and Gas Conservation Commission supplied well databases. Earthquake locations were provided by ANSS. Seismic waveforms are from the Incorporated Research Institutions for Seismology Data Management Center. N.J.v.d.E. was supported by U.S. National Science Foundation (NSF) grant EAR-1144503. H.M.S. and G.A.A. were partially supported by U.S. Geological Survey (USGS) National Earthquake Hazards Reduction Program (NEHRP) grant G13AP00024. K.M.K. received support from USGS NEHRP grant G13AP00025. This project made use of EarthScope’s Transportable Array, a facility funded by NSF. The enhanced seismicity catalogs are available as supplementary materials on Science Online.

#### Supplementary Materials

www.sciencemag.org/cgi/content/full/341/6142/164/DC1  
Materials and Methods  
Supplementary Text  
Figs. S1 to S5  
Tables S1 to S5  
References (27–43)  
Database S1

9 April 2013; accepted 23 May 2013  
10.1126/science.1238948



## Supplementary Material for

### **Enhanced Remote Earthquake Triggering at Fluid-Injection Sites in the Midwestern United States**

Nicholas J. van der Elst,\* Heather M. Savage, Katie M. Keranen, Geoffrey A. Abers

\*Corresponding author. E-mail: [nicholas@ldeo.columbia.edu](mailto:nicholas@ldeo.columbia.edu)

Published 12 July 2013, *Science* **341**, 164 (2013)

DOI: [10.1126/science.1238948](https://doi.org/10.1126/science.1238948)

**This PDF file includes:**

Materials and Methods

Supplementary Text

Figs. S1 to S5

Tables S1 to S5

References (27–43)

**Other Supplementary Material for this manuscript includes the following:**

(available at [www.sciencemag.org/cgi/content/full/341/6142/164/DC1](http://www.sciencemag.org/cgi/content/full/341/6142/164/DC1))

Database S1 as separate Excel file

## Materials and Methods

### Triggering detection: matched filter

A matched filter is used as an event detector in continuous waveforms at each of the TA stations to identify un-cataloged earthquakes. In this approach, we start with a set of seismograms from earthquakes known to have occurred in the region of interest, either identified on high-pass filtered seismograms or taken from the ANSS catalog. These seismograms are stacked to produce a template (Fig. S1), which is then cross-correlated with the entire continuous recording at a given station. Spikes in the cross-correlation score correspond to likely earthquakes in the target location. This lets us search quickly and efficiently for earthquakes that may have been too small to register on the multiple seismic stations required to obtain a catalog location.

We use the matched filter as a candidate event detector, and do not use cross-correlation scores alone to assign detections. We design the detector to admit some range in waveform similarity, as we want to detect any events within +/- several kilometers relative to the template events. We find the greatest success using a relatively high-frequency band-passed template (8-12 Hz), with a relatively long duration (10 – 20 seconds), where success is subjectively defined as a high number of candidate detections, a manageable proportion of false positives, and reasonable computation time. At these frequencies the template largely reflects scattered energy. The long duration of the template means that any signal showing a low amplitude P-wave with a sudden step to a higher amplitude S-wave (with the appropriate polarity) tends to show up in the detector function. Candidate detections are those with a cross-correlation score greater than 5 standard deviations above the noise level, and are all visually confirmed, except where mentioned below.

We apply the matched filter to a single station at a time, due to the sparseness of stations in the regions of interest. This method has previously been used to look at induced seismicity in Texas (15). With the single-station approach it is impossible to automatically distinguish between spatially separated families of events using the correlation function alone. Instead, we sort out spatially distinct earthquakes (and remove spurious detections and quarry blasts) by visually reviewing every detection and measuring the S-P time. This allows us to accurately measure the radial distance from the station, but not to precisely determine the azimuth.

The stations used in this study are mostly from the Earthscope Transportable Array (TA), which was fortuitously present for the three cases of induced seismicity studied here (Table S3). This study would have been much more difficult or impossible without high-quality continuous stations located nearby the swarms. However, due to the evolving structure of the TA deployment, there is sometimes no single station operating throughout the entire period of interest, resulting in an evolving detection capability with time. For the Oklahoma earthquakes, no single station is operating for the entire duration of the seismicity between the Feb 2010 Maule earthquake and the first Nov 2011 M5.0 Prague main shock, and we use multiple overlapping records to complete the time period.

The templates are designed using either the known times of cataloged earthquakes, or events detected on high-pass filtered waveforms in the several days around a trigger event or main shock. For example, the template for station TA.V34A, in Oklahoma, was constructed from visually identified events in a two-day window after the Feb 2010 Maule earthquake. We bandpass the waveforms between 8 and 12 Hz, pick the S-wave arrivals, and then align the traces by cross-correlation of a +/- 1 second window around the S-wave arrival. Finally, the traces are stacked to produce the template (Fig. S1). In Oklahoma, we achieve satisfactory detector performance using a stack of all three broadband components to build the final template, while in Texas and Colorado we use a single horizontal component.

#### Auto picker for station TA.T25A

The matched filter at station TA.T25A, near Trinidad, turns up ~10,000 detections in the months after the 23 Aug 2011 M5.3 Trinidad earthquake – too many for visual analysis. Except for the +/-30 days around the 2012 Sumatra earthquake, we do not review and manually measure the S-P times of these earthquakes, and they are not included in any of the statistical analyses. However, in order to get a general picture of the activity, we use an auto-picker and a linear discriminant analysis to assign S and P-wave times to these detections (Fig. S2). We use a simple AIC picker (27, 28) to find both P and S arrival times in the high-pass filtered waveforms (corner 8 Hz), using the cross-correlation detection time as the starting guess for the S-wave pick. The AIC picker allowed to search within a +/-1 second window in order to get an estimate of the pick robustness, as discussed below. The P-wave arrival is assumed to fall within a 2-10 second window prior to the S-pick.

A linear discriminant analysis is then used to classify picks as reliable or spurious (29). In this approach, one defines a vector of measurements on the data (e.g. signal to noise ratio) that differs for real and spurious events. Our classification vector consists of the AIC scores of the P and S picks, the difference between the AIC picker and cross-correlation S-wave pick times, and the cross-correlation coefficient itself. An optimal set of coefficients for a linear combination of these measurements can then be found from a training sample (we use algorithm *ClassificationDiscriminant* from the Matlab Statistics toolbox). The hand-picked interval before the M5.3 Trinidad main shock is used as the training interval. We adjust the cost function (i.e. the relative penalty for missing a known event vs. including a spurious event) until the spurious detection rate is less than 7%, and the missed detection rate is less than 20%.

#### Other detectors: STA/LTA

One of the stations, AG.WHAR in Arkansas, is too close to the Guy seismic swarm for a matched-filter detector to be effective. The back azimuth to the earthquakes from the Guy swarm varies by almost 180 degrees, and it would be necessary to define a number of templates in order to detect events from all locations in the ~10 km long swarm. Instead, we use a less refined short-term average/long-term average filter to detect all candidate events. We use a short and long-term window of 1 and 15 seconds, respectively, and set a threshold at 4 times the standard deviation for a noise segment. This technique results in significantly more spurious detections than the matched filter,

and we visually review every event in the time window of interest ( $\pm 5$  days) to make a catalog of confirmed detections.

#### Magnitude and distance calculations

The time between the arrival of the S and P waves scales approximately linearly with distance over small distance ranges. The move-out velocity  $V_{S-P} = (1/V_S - 1/V_P)^{-1}$ . Using the known catalog locations for calibration, we find move-out velocities between 7.7 and 8 km/s for different stations and regions, corresponding to  $V_S = 3.3 - 3.4$  km/s over a typical ray path. Each set of detections is inspected to identify a distinct cluster of S-P times that defines the swarm of interest. The range of S-P times used to define each swarm varies depending on the geometry of the swarm with respect to the station and the presence of other known seismicity in the region.

Magnitudes are estimated from peak amplitudes, measured in a 4-second window after the S-wave arrival on 8 Hz high-passed waveforms to remove long-period noise. We assume that a factor of 10 difference in amplitude corresponds to one unit of difference in magnitude, and use cataloged earthquakes of known magnitude to calibrate the amplitude measurements. When there is a relatively large range of distances, e.g. Trinidad CO (Fig. S2), we also use a least squares fit to the log-amplitude vs. log-distance scaling to correct for the distance dependence.

#### Estimation of statistical significance

In the main text we report statistical significance using a simple binomial test, which treats each observed earthquake as an independent event with equal probability of falling before or after the trigger. This test makes no additional assumptions about the underlying probabilistic distribution of the event count. In Table S2 we also report a test that treats the total number of observed events as the realization of a random Poisson process, i.e. we calculate the significance of the observed rate change factor using total number of observed events as an estimate of the intensity (average rate).

We also compute the magnitude of completeness  $M_c$  for each enhanced catalog (Table S2). This is relevant for comparing the triggering signal between disparate regions. We compute  $M_c$  by the method of maximum curvature (30). This method equates  $M_c$  with the peak in the discrete frequency-magnitude distribution for each enhanced catalog. Aside from a smoothing parameter of 0.5 magnitude units, the method is non-parametric, and assumes only that the true number of events should decrease as a function of increasing magnitude. Applying a cutoff at  $M_c$  slightly affects the statistical significance assessments for some of the marginal cases.

#### Surface wave strains resolved on target faults

We looked at the triggering response to the 27 Feb 2010  $M_w$  8.8 Maule; 11 Mar, 2011  $M_w$  9.1 –Tohoku-oki, and 12 Apr, 2012  $M_w$  8.6 Sumatra earthquakes. These three remote trigger earthquakes were chosen because they generated large surface waves with strains above  $10^{-7}$  at periods of 10-100 seconds across the Midwestern United States. Shaking of this amplitude is known to trigger earthquakes in a variety of tectonic

environments (10, 20, 31-33) These are the largest strains in this frequency band by almost an order of magnitude, over the last 4 years.

We interpret varying responses to the three large trigger earthquakes as reflecting local conditions in the injection fields. An alternative hypothesis would be that the three triggers generated different strain amplitudes resolved on the faults, and therefore had varying triggering power. We evaluate the relative triggering power of each trigger by resolving the dilatational and Coulomb strain components on each fault. We find no systematic differences between the amplitudes of surface waves that did or did not trigger seismicity at each of the injection sites.

Using focal solutions from the USGS/SLU database, we select the nodal planes most consistent with cataloged aftershock locations. At Prague, we use the trend of the relocated seismicity (4) to define the fault strike. Waveforms at Prague, OK, are taken from station TA.TUL1, those for Snyder, TX, are taken from station TA.ABTX, and those for Trinidad, CO, are from station TA.T25A, downloaded through IRIS Web Services. We remove the instrument-response and filter between 1 and 100 seconds. We use the method described in *Miyazawa and Brodsky* (34) (attributed to (35) to correct the observed surface Rayleigh wave component to 5 km depth, and to estimate the vertical strains. For the Rayleigh wave correction, we assume a half space p- and s-wave velocity of 8.7 and 5.0 km/s, respectively, and a group velocity of 3500 m/s (note that these velocities represent the averages over the Rayleigh wave sensitivity kernel, and not the local velocities at 5 km depth). The Love wave correction at these shallow depths is negligible (<1%) and we neglect it in calculating the shear and normal tractions on the vertical strike slip faults. In the case of the normal-faulting Trinidad main shock, the peak shear traction in the down-dip direction is carried by the Rayleigh wave, as the transverse components for the remote earthquakes are all sub-parallel to the fault strike.

The Coulomb strain  $\varepsilon_r - \mu(\varepsilon_n - B\bar{\varepsilon})$  is calculated using a coefficient of friction  $\mu = 0.6$ , and a Skempton's poro-elastic coefficient  $B = 0.8$ . The angles of incidence between the surface waves from the three triggers and the three target faults are all relatively similar (Table S5), and changing the parameters values does not significantly alter the relative magnitudes of the Coulomb strain.

## **Supplementary Text**

### Geology and pumping history of the Study Areas Snyder, TX

Snyder, Texas, has a history of seismicity associated with subsurface fluid injection. The area is part of the Horseshoe Atoll, a series of large carbonate reef reservoirs. In 1978, earthquakes up to  $M_L 5.3$  (ANSS) occurred in the Cogdell field, induced by waterflooding as part of secondary oil recovery, which began ~20 years prior to the onset of seismicity (8). Waterflooding and CO<sub>2</sub> injection for secondary recovery continue today in the Cogdell field, now along with the disposal of wastewater and CO<sub>2</sub> [Texas Railroad Commission]. Injection rates for the field as a whole have remained fairly constant or increased slightly since the late 1980s (Fig. S3). After the earthquakes in the late 1970s to mid 1980s, the Cogdell field had a period of relative quiet, with no earthquakes from

1986-2005 and five earthquakes between 2006-2009 (ANSS catalog). In 2010, seismicity rates increased dramatically to 10/yr. This recent activity is within the same injection field as the 1970s events, within the accuracy of the ANSS catalog. The rate continued to increase until an M4.5 earthquake on 11 Sept 2011, the largest to occur in this latest sequence. Seismicity has decreased in the area near the Cogdell field since this event.

The Cogdell oil fields are located within a larger ancient carbonate platform (36). The Horseshoe Atoll is a carbonate reservoir within this larger structure that accumulated in the Late Paleozoic. Surveys of the nearby Diamond-M field have shown that the Canyon Reef formation is highly compartmentalized (36) associated with lateral variations within the reef. Waterflooding for secondary oil recovery into the Canyon Reef Formation is a typical practice for this area.

### Prague, OK

Oklahoma has a long history of oil and gas extraction, and underground disposal of associated fluids has been taking place in the Wilzetta fields near Prague for nearly 20 years (OK Corp. Commission). Oklahoma has historically produced a small but steady trickle of cataloged earthquakes, with ~1.7 M3.0 or larger earthquakes recorded per year since 2002 in the ANSS catalogs. This changed dramatically in 2009 and 2010 when the number jumped to 31/yr (37). Earthquake rates increased until November 2011, when Prague was struck by three M5.0 and larger earthquakes in four days. The aftershock sequences of these events define three rupture planes that extend to within ~200 meters of two of the disposal wells, strongly suggesting that these earthquakes were induced (4).

The geology in the Prague area consists of mostly sandstones, shales and carbonates. The area has been actively extracting hydrocarbons since the 1940s. Many of the oil fields are broken up into isolated pockets, where the producing regions are isolated laterally from non-producing regions by impermeable faults, as evidenced by non-producing wells surrounding these pockets (4, 38). Vertical movement of hydrocarbons is limited by impermeable shale layers. Wastewater disposal into an isolated pocket near Prague began into the Hunton and Arbuckle formations in the 1990s at very low volume and zero wellhead pressure. Pressures were incrementally increased, until 2006 when they reached their peak of ~3.5 MPa. Pressures were halved in 2011. Seismicity in the region did not begin until 2010, as discussed in this paper.

### Trinidad, CO

The Raton Basin near Trinidad, Colorado is an active coal bed methane field where a swarm of felt earthquakes occurred in 2001, including an M4.6 (39). The rate of M3.0 and greater earthquakes in the field has increased drastically since 2001 from about 1 every 6 years prior to 2001 to 1 every 20 days between Jan. 2009 and Jan. 2011 (Fig. S3). In Aug. 2011, the Raton basin experienced an earthquake swarm that included a M5.3 (7). Increasing evidence suggests that most of the seismicity in this region is related to industrial activities (7).

There are at least five active injection wells within 10 km of the catalog epicenter, most of which began injecting between 2000 and 2001 [Colorado Oil and Gas

Conservation Commission]. The closest well (4.5 km from the main shock) began injecting in late 2005, but increased pumping rates by almost a factor of 3 starting in Jan. 2009 (Fig. S3). Three other wells within 7.8 to 8.5 km of the M5.3 main shock also increased pumping rates in Jan. 2009, including one that increased injection volumes to ~650 m<sup>3</sup> per day after a 4-year hiatus. This rapid increase in fluid volume in 2009 may have caused fluid pressure to increase in surrounding formations and along faults.

The Raton Basin is a Cretaceous-aged syncline that formed during the Laramide Orogeny. The western limb of the syncline is steeply dipping to overturned. The eastern side is very shallowly dipping (3 degrees) (40, 41). The Raton Basin has been an active area of coal bed methane exploration for decades, with most of the natural gas extraction taking place in the Raton and Vermejo sandstones (41). Wastewater injection began in the late 1980s and injects mostly into the Purgatoire and Dakota Formations, as well as the Niobrara, Entrada and Glorieta Formations (39) [Colorado Oil and Gas Conservation Commission]. The Purgatoire Formation consists of sandstone, shale and coal beds, whereas the Dakota Formation consists mostly of evenly bedded shales and sandstones (40). These formations are immediately overlain by the Pierre Shale, which is thought to be an aquatard, although fractures within the shales might allow fluid flow (42). Injection into almost all wells requires zero wellhead pressure (39).

#### Detailed analysis of triggering at Trinidad, CO

The Feb 2010 Maule earthquake triggered four small events near the Trinidad main shock (Labeled 'A' in Fig. S2). It may also have triggered a separate burst located ~5 km closer to station TA.T25A than the M5.3 main shock epicenter and consistent with its rupture zone (Labeled 'B' in Fig. S2). This burst consisted of ~30 events between 11 and 12 days after the Feb 2010 Maule earthquake (Fig. 4C). While this burst is suggestive of triggering along the eventual rupture zone, the delay and the spatial separation from the epicenter make it difficult to establish a definitive triggering link for this particular subset. The Apr 2012 Sumatra earthquake triggered a sequence consistent with the distance to the far edge of the swarm, where activity had not been very high, prior (Labeled 'C' in Fig. S2). According to the model discussed in the main text, such triggering at the margins of the swarm may indicate that fracture permeability in these marginal regions is not yet dominated by local microseismicity, allowing them to respond to permeability enhancement by transient stresses.

#### Regions of active intraplate or induced seismicity with no observed triggering Jones, OK

A prominent ongoing swarm has occurred near Jones, OK, ~50 km west of the Prague sequence (Fig. S4), starting in 2008. While we do not know the relationship, if any, between these earthquakes and injection or extraction activities, we include this cluster because of its proximity to active disposal and production fields. We construct a template for the Jones swarm using stations TA.V34A and OK.FNO. The Jones region had a number of earthquakes up to M3.9 in 2009 and 2010. Taking only detections with S-P times less than 7 seconds at both stations excludes the Prague swarm (Fig. S4). The swarm in Jones, OK, does not respond to the Feb 2010 Maule, or Apr 2012 Sumatra earthquakes (Fig. S4, Table S4). For the Mar 2011 Tohoku-oki earthquake, the case is

more equivocal. The 10-day statistics appear significant, with 2 events prior and 15 events after (Table S4). However, the rate increase follows the timing of the trigger by 4 days, whereas all the other triggering signals in the main text begin with 1 day. Also unlike any of the triggering signals in the main text, the significance is predominantly due to a relative lull in the 10 days prior. The rate of earthquakes 4 days after the trigger is consistent with the longer-term average over the 10-30 days prior to the trigger. Nevertheless, the Jones region warrants continued monitoring over the next several years.

### Guy, Arkansas

Guy, Arkansas had a prominent swarm from Sept 2010 to Apr 2011, including earthquakes up to M4.7, but shows no response to either the Feb 2010 Maule earthquake, which preceded the swarm by 7 months, or the Mar 2011 Tohoku-oki earthquake, which occurred during the peak of swarm activity (Table S4). Pumping has occurred within 10's of kilometers of the swarm location since at least 2009, at relatively high pressures (>10 MPa) (3). However, the wells most closely associated with the ensuing swarm began pumping in Aug 2010, preceding the onset of seismicity by only a month. Intense swarm activity eventually prompted a shut-down of these wells on 3 Mar 2011. Nearby pumping therefore had not begun at the time of the Feb 2010 Maule earthquake, and had ceased by the time of the 11 Mar 2011 Tohoku-oki earthquake.

Station NM.UALR was the closest station during the 27 Feb 2010 Maule earthquake. The sensitivity of this station is somewhat poor, with only a few more events detected than are present in the ANSS catalog. No rate increase is observed.

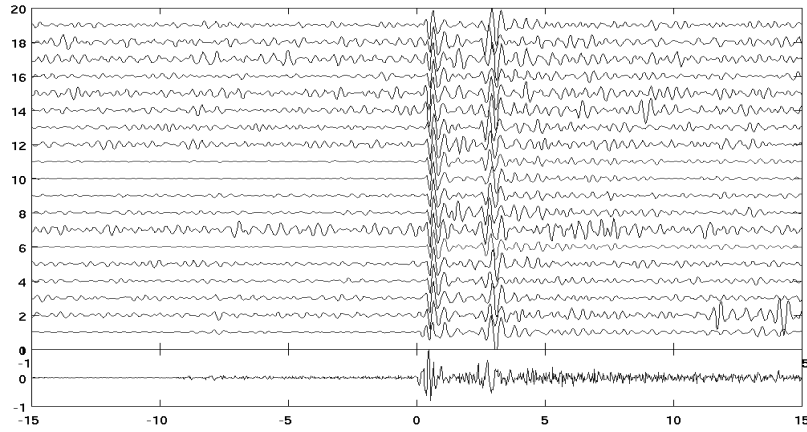
The closest station operating during the 11 Mar 2011 Tohoku-oki earthquake, AG.WHAR, is located only ~1 km from the closest earthquakes of the Guy swarm, which extends approximately 10 km to the NE and SW. This is too close for a correlation-based detector, which requires a relatively similar path between all candidate events and the station. We use a simple STA/LTA detector instead, and focus on the +/-5 days around the Tohoku-oki earthquake. As with the cross-correlation detector, each candidate event is visually reviewed, and only earthquakes with S-P times less than 1.5 seconds are retained. We also take care not to include potential quarry blasts, recognizable by their large Lg components relative to the P and S wave amplitudes. The Guy swarm shows no response to the Mar 2011 Tohoku-oki earthquake (Fig. S5), but instead shows a gradual decrease in rate that reflects the shut-down in pumping 8 days prior.

### Youngstown, Ohio

The Youngstown earthquake swarm of 2011-2012, which included an M4.0 earthquake on Dec. 31 2011, occurred under circumstances similar to those in Arkansas, with pumping at associated wells beginning in Jan. 2011, only 11 days before the first observed seismicity, and being shut down several months before the occurrence of the Apr. 2012 Sumatra earthquake. A single-station correlation detector has already been used to study un-cataloged earthquakes at the Youngstown site (5). There are 8 earthquakes detected in the 10 days after the Mar 2011 Tohoku-oki earthquake, relative to 4 prior (Kim, personal communication). This increase has a 19% probability of being observed by chance (Table S4). The earthquakes in the 10 days prior are relatively small

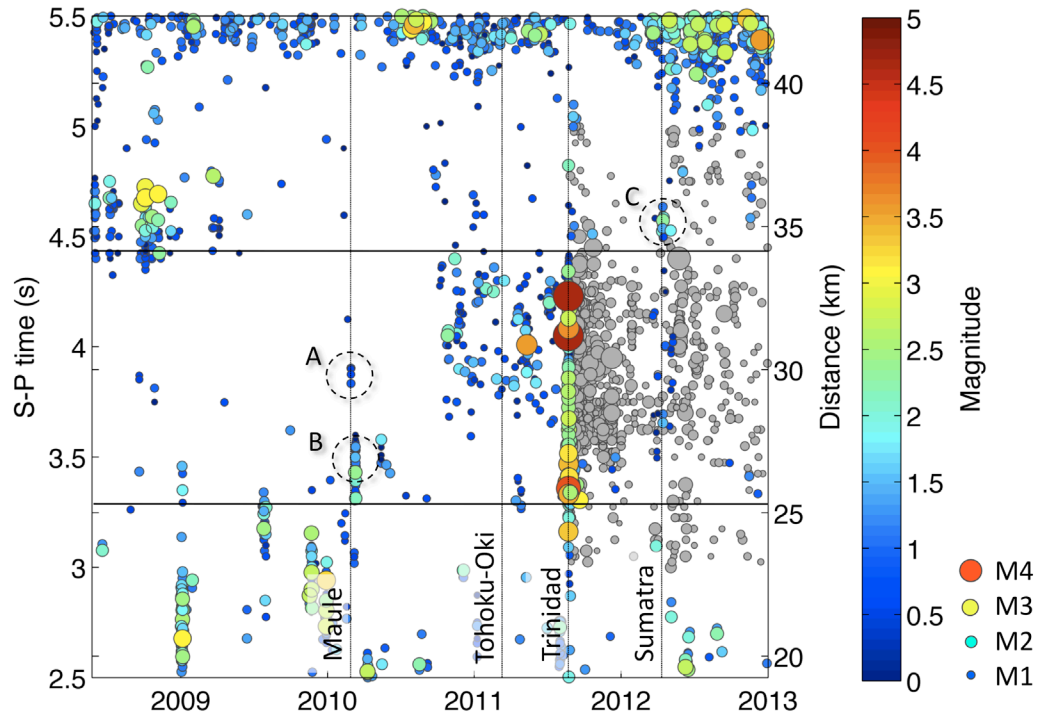
in magnitude, and applying a cutoff at the magnitude of completeness ( $M_c = 0.8$ ) results in a probability estimate of 4%. The results at Youngstown are therefore suggestive, but inconclusive. None of the 8 post-trigger earthquakes fall within 24 hours of the Tohoku-oki earthquake seismic waves.

**Fig. S1.**



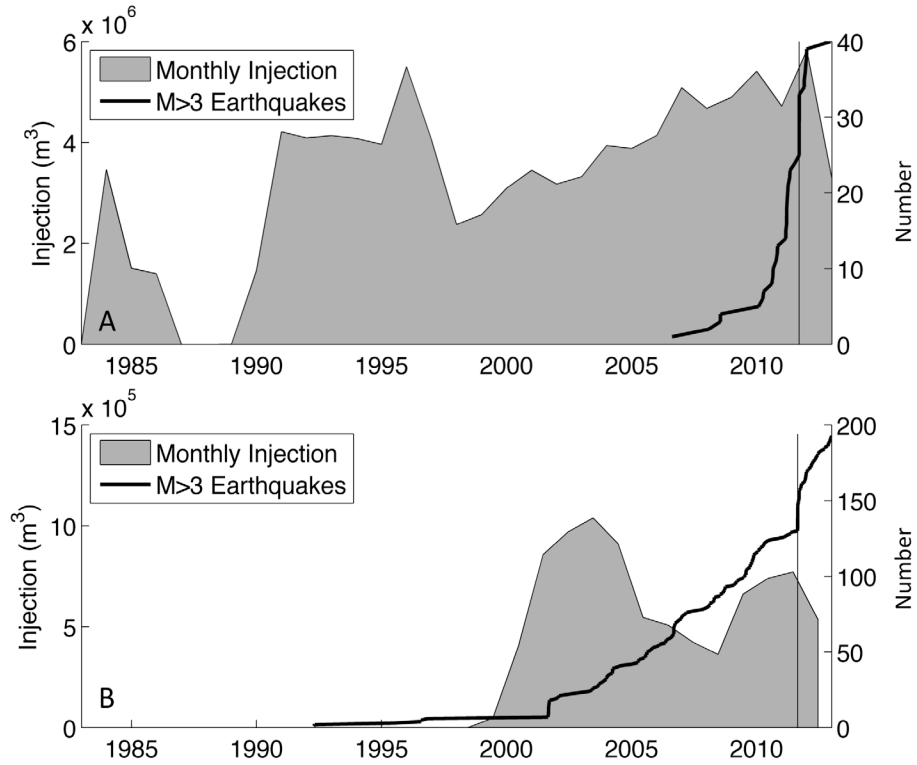
**Fig S1.** Example template for station TA.V34A constructed from earthquakes triggered by the 2010 Maule earthquake near Prague, OK. The bottom trace shows a representative high-pass filtered event (8Hz), showing the P-wave arrival at -9.6 seconds. A strong basin reverberation comes in at 2.5 seconds after the S-wave arrival.

Fig. S2



**Fig. S2.** Map of S-P times (distance) for matched-filter detections at station TA.T25A, showing the rise in activity between 25-35 km distance in Oct. 2010, leading up to the 2011 Trinidad earthquake swarm. Grey circles are auto-picked detections, and have not been reviewed. Horizontal lines show the range of S-P times plotted in Fig. 5, main text. Labels ‘A’, ‘B’, and ‘C’ mark bursts of triggered earthquakes (SM text).

**Fig. S3**



**Fig S3.** Pumping and seismicity histories for triggered locations. (A) Snyder, Texas. Total Cogdell oilfield injection by month, (courtesy C. Frohlich), showing late onset of seismicity. Most of the Cogdell oil field wells are within 10 km of the M4.5 Snyder earthquake epicenter. (B) Pumping history for the Raton basin, for 5 deep injection wells within 10 km of the M5.4 Trinidad earthquake epicenter (API 05-071-07035, 05-071-06946, 05-071-07455, 05-071-06741, and 05-071-06421). Data are available from [cogcc.state.co.us](http://cogcc.state.co.us). For injection history near Prague, Oklahoma, see *Keranen et al.* (4).

**Fig. S4**

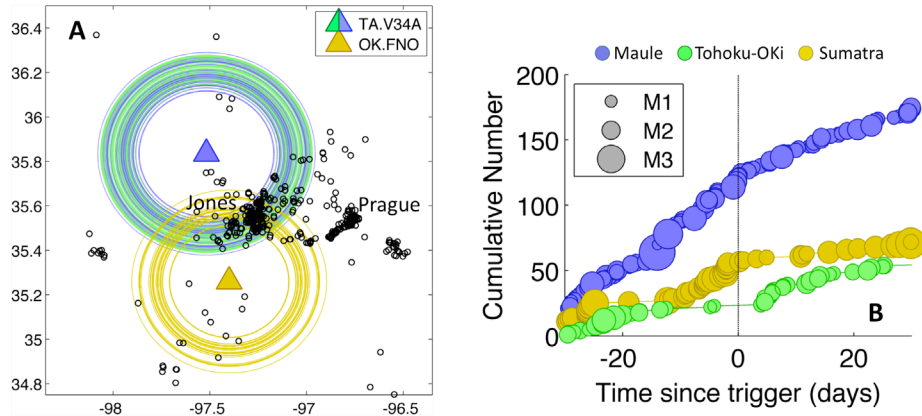


**Fig S4.** Matched-filter enhanced catalog for Jones, Oklahoma. No triggering is evident for this ongoing swarm region, 50 km west of Prague, OK. **(A)** Matched-filter detection distances for the Jones swarm region. Black circles show ANSS earthquake locations. **(B)** Count of detections for the Jones region, over the +/-30 days around three potential triggers earthquakes: Feb 2010 Maule, Mar 2011 Tohoku-oki, Apr. 2012 Sumatra.

**Fig. S5**

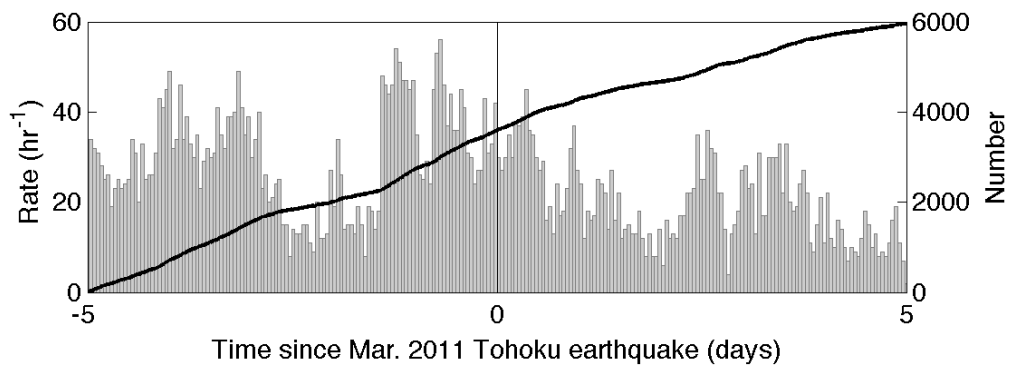


**Fig. S5.** Filtered-waveform enhanced catalog at Guy, Arkansas. No triggering is evident in the rate of earthquakes recorded at station AG.WHAR, 1 km from the Guy Arkansas swarm, from high-pass filtered waveforms. Time is relative to the Tohoku-oki earthquake, approximately 8 days after pumping has stopped at nearby wells.

**Table S1.**

Locations of all M4.5 or larger earthquakes in the mid-continental United States between 1-Jan-2003 and 1-Jan-2013 (ANSS catalog).

<b>Location</b>	<b>Date</b>	<b>ANSS Magnitude</b>	<b>Field/Formation</b>	<b>Reference<sup>†</sup></b>
New Madrid SZ*, AL	2003-04-29	4.6	-	-
Raton, NM	2005-08-10	5.0	Raton Basin	<i>Meremonte et al., 2002</i>
Wabash SZ*, IL	2008-04-18	5.2	-	-
Wabash SZ*, IL	2008-04-18	4.7	-	-
Guy, AR	2011-02-28	4.7	Fayetteville Shale	<i>Horton, 2012</i>
Trinidad, CO	2011-08-22	4.7	Raton Basin	<i>Meremonte et al., 2002</i>
Trinidad, CO	2011-08-23	5.4	Raton Basin	<i>Meremonte et al., 2002</i>
Snyder, TX	2011-09-11	4.5	Cogdell	<i>Davis and Pennington, 1989</i>
Prague, OK	2011-11-05	5.0	Wilzetta	<i>Keranen et al., 2013</i>
Prague, OK	2011-11-06	5.7	Wilzetta	<i>Keranen et al., 2013</i>
Prague, OK	2011-11-08	5.0	Wilzetta	<i>Keranen et al., 2013</i>
Timpson, TX	2012-05-17	4.8	Haynesville Shale	<i>Brown et al., 2012</i>

\*SZ: Seismic Zone

<sup>†</sup>Reference suggesting link between named field and historical or recent induced earthquakes.

**Table S2.**

Statistical significance of observed rate changes in triggered regions

Location	Catalog/ Station *	Remote Trigger	Num. before <sup>†</sup>	Num. after <sup>†</sup>	$M_c$	Binomial <sup>‡</sup>		Poisson <sup>‡</sup>	
						$p$	$p_c$	$p$	$p_c$
Midwest <sup>§</sup>	ANSS	Stack	4	12	3.0	<b>0.04</b>	<b>0.04</b>	<b>0.03</b>	<b>0.03</b>
Snyder, TX	TA.130A	Maule	3	3	1.1	0.66	0.81	0.58	0.69
	TA.ABTX	Tohoku	1	8	2.6	<b>0.02</b>	<b>0.02</b>	<b>0.02</b>	<b>0.05</b>
	TA.ABTX	Sumatra	0	0	2.6	-	-	-	-
Prague, OK	TA.V34A	Maule	0	51	1.0	<b>10<sup>-16</sup></b>	<b>10<sup>-16</sup></b>	<b>10<sup>-16</sup></b>	<b>10<sup>-16</sup></b>
	TA.V35A	Tohoku	0	1	1.3	0.50	0.50	0.61	0.61
	OK.FNO	Sumatra	0	6	2.4	<b>0.02</b>	0.13	<b>0.05</b>	0.22
Trinidad, CO	TA.T25A	Maule	1	4 <sup>¶</sup>	0.4	<b>10<sup>-4</sup></b>	<b>10<sup>-4</sup></b>	<b>0.01</b>	<b>0.01</b>
	TA.T25A	Tohoku	4	2	0.4	0.89	0.81	0.82	0.69
	TA.T25A	Sumatra	2	7	0.4	0.09	0.06	0.06	<b>0.05</b>

\*Station counts from matched-filter enhanced catalogs

<sup>†</sup>10-day window

<sup>‡</sup>A low probability indicates a stronger potential triggering signal. Columns marked  $p_c$  use only events about  $M_c$ . Grey rows are significant above 95% confidence for all tests. The Binomial test treats the number of events as fixed, while the Poisson probability treats the observed number of events itself as a realization of a random variable. A continuous approximation of the Poissonian probability density function is used.

<sup>§</sup>Excluding Guy, Arkansas due to active induced swarm (See below)

<sup>¶</sup>The 10-day binomial test has insufficient power if the number of triggered events is fewer than 5. Significance in this case is computed using a post-trigger window of 1 day.

**Table S3:**

Stations used to construct matched filter catalogs.

Station	Location	Start time	End time	Region	Distance (km) <sup>*</sup>	SP time range (s)	Potential Triggers <sup>†</sup>
TA.V34A	N35.83 W97.52	2009/10/31	2011/09/03	Prague	65	9.0 - 9.7	M T -
				Jones	40	4.2 - 7.2	
TA.V35A	N35.76 W96.84	2010/03/13	2012/02/20	Prague	24	3.5 - 4.0	- T -
TA.TUL1	N35.91 W95.79	2008/10/16	N/A	Prague	180	N/A	M T S
OK.FNO	N35.26 W97.40	2011/10/10	N/A	Prague	67	7.7 - 8.7	- - S
				Jones	39	3.5 - 6.0	
TA.ABTX	N32.62 W99.64	2009/02/12	N/A	Snyder	113	14 - 15.5	M T S
TA.130A	N32.60 W100.97	2009/03/12	2011/02/09	Snyder	36	3.5 - 5.5	M - -
TA.T25A	N37.14 W104.41	2008/05/25	N/A	Trinidad	27	3.5 - 4.5	M T S
NM.UALR	N34.78 W92.34	1999/06/22	N/A	Guy	59	5.9 - 8.5	M - -
AG.WHAR	N35.29 W92.29	2010/05/17	N/A	Guy	1.5	0.1-1.5	- T S

<sup>\*</sup>Distance between station and target triggered events.<sup>†</sup>M: Feb 2010 Maule; T: Mar 2011 Tohoku-oki; S: Apr 2012 Sumatra

**Table S4:**

Statistical significance of observed rate changes in other selected regions

Location	Catalog/ Station*	Remote Trigger	Num. before <sup>†</sup>	Num. after <sup>†</sup>	$M_c$	Binomial		Poisson	
						$P$	$P_c$	$P$	$P_c$
Jones, OK	TA.V34A	Maule	33	25	1.3	0.88	0.87	0.96	0.83
	TA.V34A	Tohoku	2	15	1.3	<b><math>10^{-3†}</math></b>	<b><math>10^{-3†}</math></b>	<b><math>10^{-3†}</math></b>	<b><math>10^{-3†}</math></b>
	OK.FNO	Sumatra	26	10	2.2	1.00	1.00	1.00	1.00
Guy, AR	NM.UALR	Maule	4	1	1.5 <sup>‡</sup>	0.97	-	0.90	-
	AG.WHAR	Tohoku	3594 <sup>§</sup>	2363 <sup>§</sup>	-	1.00	-	1.00	-
Youngstown, OH	TA.T25A	Tohoku	4	8	0.9	0.19	0.06	0.16	<b>0.05</b>

\*10-day window

<sup>†</sup>Significance is attributed to unusually low rates in the previous 10 days and is inconclusive (see text)<sup>‡</sup>5-day window. Magnitudes were not systematically calculated for this station.<sup>§</sup> Too few events were detected to establish completeness. We use the average completeness level found for stations at ~60km from Prague, instead, which leaves zero events before and after.

**Table S5:**

Remote trigger earthquakes and resolved strain at each triggered site.

Site	Trigger	Distance	Back	Strike	Dip	Peak	Peak	Triggering
			Azimuth			Dilation	Coloumb	
						[ $\mu$ strain]	[ $\mu$ strain]	
Snyder,	Maule	74°	156°	30	90*	0.22	0.22	No
TX	Tohoku	89°	316°			0.24	0.16	Yes
	Sumatra	143°	339°			0.11	0.20	No
Prague,	Maule	75°	160°	34	90*	0.25	0.25	Yes
OK	Tohoku	89°	319°			0.29	0.20	No
	Sumatra	141°	347°			0.16	0.23	Some
Trinidad,	Maule	79°	153°	21	53†	0.22	0.33	Yes
CO	Tohoku	83°	313°			0.24	0.34	No
	Sumatra	137°	334°			0.11	0.15	Some

\*Peak Coulomb strain carried by Love wave component.

†Peak Coulomb strain carried by Rayleigh wave component.

**Additional Data Table S1 Caption**

Matched-filter enhanced catalogs for each station in Table S3, containing detection times in Matlab and calendar formats, magnitude, and S-P times of all detected events.

## References and Notes

1. C. B. Raleigh, J. H. Healy, J. D. Bredehoeft, An experiment in earthquake control at Rangely, Colorado. *Science* **191**, 1230–1237 (1976). [doi:10.1126/science.191.4233.1230](https://doi.org/10.1126/science.191.4233.1230) [Medline](#)
2. National Research Council, *Induced Seismicity Potential in Energy Technologies* (National Academies Press, New York, 2012).
3. S. Horton, Disposal of hydrofracking waste fluid by injection into subsurface aquifers triggers earthquake swarm in central Arkansas with potential for damaging earthquake. *Seismol. Res. Lett.* **83**, 250–260 (2012). [doi:10.1785/gssrl.83.2.250](https://doi.org/10.1785/gssrl.83.2.250)
4. K. M. Keranen, H. M. Savage, G. A. Abers, E. S. Cochran, Potentially induced earthquakes in Oklahoma: Links between wastewater injection and the 2011 Mw 5.7 earthquake sequence. *Geology* **41**, 699–702 (2013). [doi:10.1130/G34045.1](https://doi.org/10.1130/G34045.1)
5. W.-Y. Kim, “Induced seismicity associated with fluid injection into deep wells in Youngstown, Ohio,” abstract S43D-2496 presented at 2012 Fall Meeting, American Geophysical Union, San Francisco, CA, 3 to 7 December 2012.
6. C. Frohlich, J. Glidewell, M. Brunt, Location and Felt reports for the 25 April 2010 m(bLg) 3.9 earthquake near Alice, Texas: Was it induced by petroleum production? *Bull. Seismol. Soc. Am.* **102**, 457–466 (2012). [doi:10.1785/0120110179](https://doi.org/10.1785/0120110179)
7. J. L. Rubinstein, W. L. Ellsworth, A. McGarr, “The 2001–present triggered seismicity sequence in the Raton basin of southern Colorado/Northern New Mexico,” BSSA Abstracts 2013 Annual Meeting 155D, (2013).
8. S. D. Davis, W. D. Pennington, Induced seismic deformation in the Cogdell Oil-Field of west Texas. *Bull. Seismol. Soc. Am.* **79**, 1477–1494 (1989).
9. R. B. Horner, J. E. Barclay, J. M. MacRae, Earthquakes and hydrocarbon production in the Fort St. John area of Northeastern British Columbia. *Can. J. Explor. Geophys.* **30**, 39–50 (1994).
10. N. J. van der Elst, E. E. Brodsky, Connecting near-field and far-field earthquake triggering to dynamic strain. *J. Geophys. Res.* **115**, B07311 (2010). [doi:10.1029/2009JB006681](https://doi.org/10.1029/2009JB006681)
11. H. M. Savage, C. Marone, Potential for earthquake triggering from transient deformations. *J. Geophys. Res.* **113**, B05302 (2008). [doi:10.1029/2007JB005277](https://doi.org/10.1029/2007JB005277)
12. D. P. Hill, S. G. Prejean, in *Dynamic Triggering*, vol. 4, H. Kanamori, Ed., Treatise on (Elsevier, New York, 2007), pp. 257 to 292.
13. D. P. Hill, P. A. Reasenber, A. Michael, W. J. Arabaz, G. Beroza, D. Brumbaugh, J. N. Brune, R. Castro, S. Davis, D. Depolo, W. L. Ellsworth, J. Gomberg, S. Harmsen, L. House, S. M. Jackson, M. J. Johnston, L. Jones, R. Keller, S. Malone, L. Munguia, S. Nava, J. C. Pechmann, A. Sanford, R. W. Simpson, R. B. Smith, M. Stark, M. Stickney, A. Vidal, S. Walter, V. Wong, J. Zollweg, Seismicity remotely triggered by the magnitude 7.3 Landers, California, earthquake. *Science* **260**, 1617–1623 (1993). [doi:10.1126/science.260.5114.1617](https://doi.org/10.1126/science.260.5114.1617) [Medline](#)
14. Materials and methods are available as supplementary materials on *Science Online*.

15. C. Frohlich, C. Hayward, B. Stump, E. Potter, The Dallas-Fort Worth Earthquake sequence: October 2008 through May 2009. *Bull. Seismol. Soc. Am.* **101**, 327–340 (2011). [doi:10.1785/0120100131](https://doi.org/10.1785/0120100131)
16. Z. G. Peng, P. Zhao, Migration of early aftershocks following the 2004 Parkfield earthquake. *Nat. Geosci.* **2**, 877–881 (2009). [doi:10.1038/ngeo697](https://doi.org/10.1038/ngeo697)
17. D. R. Shelly, G. C. Beroza, S. Ide, Non-volcanic tremor and low-frequency earthquake swarms. *Nature* **446**, 305–307 (2007). [doi:10.1038/nature05666](https://doi.org/10.1038/nature05666) [Medline](#)
18. J. E. Vidale, P. M. Shearer, A survey of 71 earthquake bursts across southern California: Exploring the role of pore fluid pressure fluctuations and aseismic slip as drivers. *J. Geophys. Res.* **111**, B05312 (2006). [doi:10.1029/2005JB004034](https://doi.org/10.1029/2005JB004034)
19. T. Parsons, A. A. Velasco, Absence of remotely triggered large earthquakes beyond the mainshock region. *Nat. Geosci.* **4**, 312–316 (2011). [doi:10.1038/ngeo1110](https://doi.org/10.1038/ngeo1110)
20. E. E. Brodsky, S. G. Prejean, New constraints on mechanisms of remotely triggered seismicity at Long Valley Caldera. *J. Geophys. Res.* **110**, B04302 (2005). [doi:10.1029/2004JB003211](https://doi.org/10.1029/2004JB003211)
21. S. Husen, R. Taylor, R. B. Smith, H. Healsler, Changes in geyser eruption behavior and remotely triggered seismicity in Yellowstone National Park produced by the 2002 M 7.9 Denali fault earthquake, Alaska. *Geology* **32**, 537–540 (2004). [doi:10.1130/G20381.1](https://doi.org/10.1130/G20381.1)
22. E. E. Brodsky, E. Roeloffs, D. Woodcock, I. Gall, M. Manga, A mechanism for sustained groundwater pressure changes induced by distant earthquakes. *J. Geophys. Res.* **108**, (B8), 2390 (2003). [doi:10.1029/2002JB002321](https://doi.org/10.1029/2002JB002321)
23. T. Taira, P. G. Silver, F. L. Niu, R. M. Nadeau, Remote triggering of fault-strength changes on the San Andreas fault at Parkfield. *Nature* **461**, 636–639 (2009). [doi:10.1038/nature08395](https://doi.org/10.1038/nature08395) [Medline](#)
24. J. E. Elkhoury, A. Niemeijer, E. E. Brodsky, C. Marone, Laboratory observations of permeability enhancement by fluid pressure oscillation of in situ fractured rock. *J. Geophys. Res.* **116**, (B2), B02311 (2011). [doi:10.1029/2010JB007759](https://doi.org/10.1029/2010JB007759)
25. T. M. Mitchell, D. R. Faulkner, Experimental measurements of permeability evolution during triaxial compression of initially intact crystalline rocks and implications for fluid flow in fault zones. *J. Geophys. Res.* **113**, (B11), B11412 (2008). [doi:10.1029/2008JB005588](https://doi.org/10.1029/2008JB005588)
26. S. Micklethwaite, S. F. Cox, Progressive fault triggering and fluid flow in aftershock domains: Examples from mineralized Archaean fault systems. *Earth Planet. Sci. Lett.* **250**, 318–330 (2006). [doi:10.1016/j.epsl.2006.07.050](https://doi.org/10.1016/j.epsl.2006.07.050)
27. N. Maeda, A method for reading and checking phase times in auto-processing system of seismic wave data. *Zisin Jishin* **38**, 365–379 (1985).
28. H. J. Zhang, C. Thurber, C. Rowe, Automatic P-wave arrival detection and picking with multiscale wavelet analysis for single-component recordings. *Bull. Seismol. Soc. Am.* **93**, 1904–1912 (2003). [doi:10.1785/0120020241](https://doi.org/10.1785/0120020241)
29. R. Di Stefano, F. Aldersons, E. Kissling, P. Baccheschi, C. Chiarabba, D. Giardini, Automatic seismic phase picking and consistent observation error assessment:

- Application to the Italian seismicity. *Geophys. J. Int.* **165**, 121–134 (2006).  
[doi:10.1111/j.1365-246X.2005.02799.x](https://doi.org/10.1111/j.1365-246X.2005.02799.x)
30. S. Wiemer, M. Wyss, Minimum magnitude of completeness in earthquake catalogs: Examples from Alaska, the western United States, and Japan. *Bull. Seismol. Soc. Am.* **90**, 859–869 (2000). [doi:10.1785/0119990114](https://doi.org/10.1785/0119990114)
  31. J. Gomberg, S. Davis, Stress strain changes and triggered seismicity at The Geysers, California. *J. Geophys. Res.* **101**, (B1), 733–749 (1996). [doi:10.1029/95JB03250](https://doi.org/10.1029/95JB03250)
  32. A. A. Velasco, S. Hernandez, T. Parsons, K. Pankow, Global ubiquity of dynamic earthquake triggering. *Nat. Geosci.* **1**, 375–379 (2008). [doi:10.1038/ngeo204](https://doi.org/10.1038/ngeo204)
  33. J. Gomberg, P. Johnson, Seismology: Dynamic triggering of earthquakes. *Nature* **437**, 830–830 (2005). [doi:10.1038/437830a](https://doi.org/10.1038/437830a) [Medline](#)
  34. M. Miyazawa, E. E. Brodsky, Deep low-frequency tremor that correlates with passing surface waves. *J. Geophys. Res.* **113**, (B1), B01307 (2008). [doi:10.1029/2006JB004890](https://doi.org/10.1029/2006JB004890)
  35. A. E. H. Love, *Mathematical Theory of Elasticity* (Cambridge Univ. Press, Cambridge, UK, 1927).
  36. C. Russian, R. Perez, K. Marfurt, O. Davogustto, H. Alzahrani, A. Small, P- and S-wave delineation of the Horseshoe Atoll, Diamond-M field, Texas USA. *Leading Edge (Tulsa Okla.)* **29**, 1108–1115 (2010). [doi:10.1190/1.3485771](https://doi.org/10.1190/1.3485771)
  37. W. L. Ellsworth *et al.*, “Are seismicity rate changes in the midcontinent natural or manmade?” BSSA Abstracts 2012 Annual Meeting (2012).
  38. H. S. K. Way, thesis, Oklahoma State University, Norman, OK (1983).
  39. M. E. Meremonte *et al.*, Investigation of an earthquake swarm near Trinidad, Colorado, August-October 2001: USGS Open File Report 02-0073, (2002).
  40. E. H. Baltz, Stratigraphy and history of Raton basin and notes on San Luis basin, Colorado-New Mexico. *AAPG Bull.* **49**, 2041–2075 (1965).
  41. G. K. Hoffman, B. S. Brister, New Mexico’s Raton Basin coalbed methane play. *N.M. Geol.* **25**, 95–110 (2003).
  42. R. Wilkins, “Hydraulic fracturing retrospective case study, Raton Basin, CO,” Environmental Protection Agency Report (2012) , pp. 94.
  43. W. A. Brown, C. A. Frohlich, W. L. Ellsworth, J. H. Luetgert, M. R. Brunt, The May 17th, 2012 M4.8 earthquake near Timpson, east Texas: Was it natural or was it induced? Abstract S531-06 presented at 2012 Fall Meeting, AGU, San Francisco, CA, 3 to 7 December (2012).